Author Manuscript

Author Manuscript

Author Manuscript

Author Manuscript

HHS Public Access

Author manuscript

Nat Microbiol. Author manuscript; available in PMC 2019 May 05.

Published in final edited form as:

Nat Microbiol. 2018 December ; 3(12): 1461–1471. doi:10.1038/s41564-018-0272-x.

Interactions between *Roseburia intestinalis* and diet modulate atherogenesis in a murine model

Kazuyuki Kasahara[1], **Kimberly A. Krautkramer**[2,3], **Elin Org**[4], **Kymberleigh A. Romano**[1], **Robert L. Kerby**[1], **Eugenio I. Vivas**[1], **Margarete Mehrabian**[4], **John M. Denu**[2,3], **Fredrik Bäckhed**[5], **Aldons J. Lusis**[4], and **Federico E. Rey**[1,*]

[1]Department of Bacteriology, University of Wisconsin-Madison, Madison, WI USA

[2]Wisconsin Institute for Discovery, Madison, WI USA

[3]Department of Biomolecular Chemistry, University of Wisconsin-Madison, Madison, WI USA

[4]Division of Cardiology, Department of Medicine, David Geffen School of Medicine, University of California-Los Angeles, Los Angeles, CA USA

[5]Wallenberg Laboratory, Department of Molecular and Clinical Medicine, University of Gothenburg, Gothenburg, Sweden

Abstract

Humans with metabolic and inflammatory diseases frequently harbor lower levels of butyrate-producing bacteria in their gut. However, it is not known whether variation in the levels of these organisms is causally linked with disease development and whether diet modifies the impact of these bacteria on health. Here we show that prominent gut-associated butyrate-producing bacteria species (*Roseburia* sp.) is inversely correlated with atherosclerotic lesion development in a genetically diverse mouse population. We use germ-free *apolipoprotein E*-deficient mice colonized with synthetic microbial communities that differ in their capacity to generate butyrate to demonstrate that *Roseburia intestinalis* interacts with dietary plant polysaccharides to (i) impact gene expression in the intestine, directing metabolism away from glycolysis and toward fatty acid utilization, (ii) lower systemic inflammation and (iii) ameliorate atherosclerosis. Furthermore, intestinal administration of butyrate reduces endotoxemia and atherosclerosis development. Altogether, our results illustrate how modifiable diet-by-microbiota interactions impact cardiovascular disease, and suggest that interventions aimed at increasing the representation of butyrate-producing bacteria may provide protection against atherosclerosis.

Users may view, print, copy, and download text and data-mine the content in such documents, for the purposes of academic research, subject always to the full Conditions of use:http://www.nature.com/authors/editorial_policies/license.html#terms

*Address for Correspondence: ferey@wisc.edu, Department of Bacteriology, University of Wisconsin-Madison, 1550 Linden Dr., Madison, WI 53706. **Correspondence and requests for materials** should be addressed to F.E.R.

Author contributions

F.E.R. conceived, designed and supervised the project. K.K. designed the project, performed most of the experiments, analyzed the results, and generated figures and tables. K.A.K. performed the PTM analysis, analyzed results, and generated the figures. K.A.R. and K.K. performed COPRO-Seq analysis. R.L.K. cultured bacterial strains. F.B. provided GF *ApoE*$^{-/-}$ mice, and E.I.V. maintained GF mouse facility. A.J.L. and M.M. conceived and performed the Ath-HMDP experiment, and E.O. generated and analyzed 16S rRNA gene data. K.K., K.A.K., R.L.K., and F.E.R. wrote the manuscript. A.J.L., M.M., F.B., and J.M.D. provided critical feedback. All authors read and agreed on the final version of the manuscript.

Competing financial interests:

The authors declare no competing financial interests.

Author Manuscript Author Manuscript Author Manuscript Author Manuscript

The distal gut of mammals harbors complex and dynamic microbial communities that are shaped by diet and host factors. These communities provide the host with a vast range of functions such as digestion of complex dietary components (e.g., plant polysaccharides), production of vitamins, maturation of the immune system, and regulation of host metabolism[1]. Dietary components that are not absorbed in the proximal intestine reach the distal gut, where they are metabolized through processes that involve trophic interactions among members of the microbial community[2]. Diets rich in plant polysaccharides accessible to microbes boost the growth of many intestinal bacteria, which have evolved complex mechanisms to efficiently breakdown and metabolize these substrates[3,4,5,6]. Consequently, relative to low-fiber diets, consumption of diets enriched in carbohydrates accessible to gut microbes is associated with increased bacterial diversity[7,8].

Gut microbial fermentation of plant polysaccharides results in the production of short chain fatty acids (SCFAs), of which acetate, propionate, and butyrate are the most prominent. Butyrate has multiple positive effects in the intestinal tract: it is the preferred energy source for the colonic epithelium and modulates gene expression, at least in part through its action as a non-competitive inhibitor of histone deacetylases (HDACs), leading to hyperacetylation of chromatin[9,10]. Butyrate also exhibits anti-inflammatory properties by inhibiting the activation of the transcription factor NF-κB (nuclear factor-kappa B), which in turn results in lower expression of inflammatory cytokines[11].

Atherosclerosis is a chronic inflammatory disease and several lines of evidence suggest that the gut microbiome modulates its development: (i) germ-free (GF) mice genetically sensitive to atherosclerosis (apolipoprotein E-deficient [$ApoE^{-/-}$] mice) develop smaller atherosclerotic lesions compared to colonized counterparts[12]; (ii) Toll-like receptors and nucleotide-binding oligomerization domain-like receptors, which recognize bacterial proinflammatory molecules have been implicated in the development of atherosclerosis[13]; and (iii) trimethylamine-N-oxide (TMAO), a host-synthesized derivative of the bacterial metabolite trimethylamine (TMA), both enhances atherosclerosis in animal models and is associated with cardiovascular risks in humans[14,15]. Furthermore, patients with symptomatic atherosclerotic plaques contain lower levels of gut bacteria predicted to generate butyrate[16].

Most human gut-associated butyrate producers are Firmicutes, with the majority belonging to clostridial clusters XIVa and IV. The most common isolates include species related to *Roseburia* spp. and *Eubacterium rectale* within cluster XIVa and *Faecalibacterium prausnitzii* within cluster IV[17]. Recent studies indicate that patients with type 2 diabetes harbor lower levels of these taxa[18,19]. Additionally, butyrate-producing bacteria are highly responsive to host diet: e.g., fecal levels of *R. intestinalis* were higher in subjects consuming resistant starch-enriched diets compared to those consuming diets low in total carbohydrate[20,21].

Despite the evidence suggesting that butyrate has anti-inflammatory effects and correlation studies that demonstrate increased levels of butyrate-producing bacteria in healthy individuals compared to those with cardiometabolic disease[16,18,19], the impact of this important group of organisms on host health has not been experimentally verified.

Author Manuscript Author Manuscript Author Manuscript Author Manuscript

Specifically, it is not known whether butyrate-producing bacteria alter susceptibility and progression of atherosclerosis. In this study we show that colonization with *Roseburia intestinalis* decreases levels of inflammatory markers and atherosclerosis in a diet-dependent manner, and demonstrate that the end-product of bacterial metabolism, butyrate, mediates these effects.

Results

Abundance of *Roseburia* sp. is inversely correlated with atherosclerotic lesion size in a genetically diverse mouse cohort.

We examined the bacterial communities in the ceca from 83 strains of mice derived from the Hybrid Mouse Diversity Panel (HMDP)[22]. These strains were made susceptible to atherosclerosis by transgenic expression of human apolipoprotein E3-Leiden and human cholesteryl ester transfer protein. Characterization of 342 F1 mice expressing both transgenes ("Ath-HMDP") exposed to a high-fat cholesterol diet for 16 weeks showed a wide range in size of atherosclerotic lesions across the different strains[22]. We performed 16S rRNA gene sequencing of fecal DNA collected from these animals and conducted correlation analysis to identify taxa associated with atherosclerotic plaque size (Supplementary Table 1). We identified a number of genera whose abundances were associated ($P<0.05$) with plaque size (Supplementary Fig. 1, Supplementary Table 2). Among them *Roseburia* ($P=0.0035$, bicor=−0.157) showed the strongest negative correlation. This is consistent with human studies[16] and suggests that butyrate-producing bacteria may inhibit development of atherosclerosis. Although total plasma cholesterol levels showed a strong positive correlation with plaque size in these mice (Supplementary Fig. 2a), the relative abundance of *Roseburia* was not correlated with cholesterol (Supplementary Fig. 2b), implying that butyrate-producing bacteria may not affect cholesterol homeostasis.

Colonization with *R. intestinalis* modulates cecal butyrate accumulation in gnotobiotic mice fed a diet with high content of plant polysaccharides (HPP).

GF mice, inoculated with specific microbes isolated from the human gut, were used to study the role of butyrate-producing bacteria *in vivo*. Two groups of 8-week old GF male *ApoE*$^{-/-}$ mice were orally gavaged with the following microbial mixtures: (i) a "core" community which included eight species that are commonly found in the human microbiota with a limited capacity to produce butyrate (*Anaerotruncus colihominis*, *Bacteroides caccae*, *Bacteroides thetaiotaomicron*, *Clostridium symbiosum*, *Collinsella aerofaciens*, *Coprococcus comes*, *Providencia stuartii*, and *Ruminococcus torques*); or (ii) the same "core" community plus *R. intestinalis* (Supplementary Table 3). All mice were fed a standard HPP chow diet (Fig. 1a), and successful transplantation of these communities was confirmed using *co*mmunity *pro*filing by *seq*uencing (COPRO-Seq) analysis (Fig. 1b). The most significant difference in the communities was the presence of *R. intestinalis*, which represented 25.1% of the fecal "core plus *R. intestinalis*" community. *C. aerofaciens* was disproportionally impacted by *R. intestinalis*, showing a ~4-fold decrease in the presence of the butyrate producer compared to core community-colonized mice (Fig. 1b, Supplementary Table 4). These effects were observed even when *R. intestinalis* was not considered as part

Author Manuscript Author Manuscript Author Manuscript Author Manuscript

of the community for the calculations (i.e., core species considered as 100% for both groups; Supplementary Fig. 3, Supplementary Table 5). Additionally, *C. comes* and *C. symbiosum* also showed lower relative abundance in the presence of *R. intestinalis* (Fig. 1b, Supplementary Table 4), however these differences disappear when *R. intestinalis* is not considered for the calculations (Supplementary Fig. 3, Supplementary Table 5).

Mice were euthanized 18 weeks after colonization, and plasma and cecal contents were collected for biochemical analyses. Colonization with the "core plus *R. intestinalis*" community resulted in a four-fold increase of cecal butyrate levels compared with the "core" community (Fig. 1c, Supplementary Fig. 4). Additionally, we observed a significant reduction of cecal acetate levels—a substrate used by some butyrate-producing bacteria including *R. intestinalis* for butyrate production[23]. Nonetheless, plasma levels of butyrate and acetate were not significantly different between these two groups of mice (Fig. 1d), suggesting rapid metabolism of butyrate in peripheral tissues such as the intestine and the liver[24]. These results demonstrate that gut microbial composition affects cecal SCFA levels, and that colonization with *R. intestinalis* increases cecal butyrate concentration in mice fed the HPP diet.

Colonization with *R. intestinalis* inhibits the development of atherosclerotic plaque formation in gnotobiotic mice fed the HPP diet.

By a variety of measures the HPP-fed "core" and "core plus *R. intestinalis*" colonized mice were indistinguishable. For example, colonization with *R. intestinalis* did not affect plasma or liver lipid profiles (Supplementary Fig. 5a, Supplementary Table 6). In contrast, evaluation of atherosclerotic lesions of the aortic sinus showed marked differences: mice colonized with *R. intestinalis* exhibited a 30% reduction of atherosclerotic lesion development compared to mice colonized with the "core" community (aortic sinus mean plaque area; $23.8\pm1.7\times10^4$ μm^2 in "core" *ApoE*$^{-/-}$ mice, $16.7\pm1.7\times10^4$ μm^2 in "core plus *R. intestinalis*" *ApoE*$^{-/-}$ mice; Fig. 2a, e). Remarkably, there was a significant negative correlation between cecal levels of butyrate and lesion size (Supplementary Fig. 5b). In contrast, plasma cholesterol levels were not associated with lesion size (Supplementary Fig. 5c).

Lipid deposition measured with Oil Red O-stained sections showed that mice colonized with *R. intestinalis* also had a reduced lipid area (Fig. 2a, f). Immunohistochemical studies of atherosclerotic lesions showed that mice colonized with the "core plus *R. intestinalis*" community developed atherosclerotic lesions that exhibited a lower number of macrophages (Fig. 2b, g) and increased levels of collagen (Fig. 2c, h), suggesting that colonization with *R. intestinalis* promoted the stability of atherosclerotic plaque. In contrast, levels of smooth muscle cells in the aortic sinus were not affected by microbial community composition (Fig. 2d, i). To further define possible *R. intestinalis*-perturbed host factors associated with reduced atherosclerotic lesions and macrophage infiltration in the aortic root, we examined mRNA levels of several inflammatory markers of atherosclerosis in the aorta. While there were no significant differences in the mRNA levels of *Il (Interleukin)-6*, *Il-1β*, *Mcp1* (Monocyte chemoattractant protein 1), and *Icam1* (Intracellular adhesion molecule 1), we detected a marked reduction in the relative mRNA levels of Tumor necrosis factor α (*Tnf-α*)

Author Manuscript Author Manuscript Author Manuscript Author Manuscript

and Vascular cell adhesion molecule 1 (*Vcam1*) associated with the presence of *R. intestinalis* (Fig. 2j). Both TNF-α and VCAM-1 have a central role in controlling inflammatory processes and atherosclerosis development independent of plasma cholesterol levels[25,26]. These results suggest that colonization with *R. intestinalis* modulates atherosclerosis by reducing aortic inflammation.

We next tested whether the athero-protective effect of *R. intestinalis* is modulated by diet. GF male *ApoE*$^{-/-}$ mice colonized with the same communities described above were fed1 a diet low in complex plant polysaccharides (LPP diet, Supplementary Fig. 6a). In contrast to the HPP-fed animals, in LPP-fed animals *R. intestinalis* represented only 0.3% of the fecal "core plus *R. intestinalis*" community (Supplementary Fig. 6b-c, Supplementary Table 7). Under this condition, *R. intestinalis* did not impact community composition or any measurement collected at the time of euthanasia, including SCFA levels and atherosclerotic lesions (Supplementary Fig. 7–8, Supplementary Table 6). Thus, the abundance and athero-protective effects of *R. intestinalis* depend on the availability of dietary plant polysaccharides.

R. intestinalis modulates intestinal epigenetic programing in the colon of mice fed the HPP diet.

Mice colonized with *R. intestinalis* that were fed the HPP diet showed increased butyrate levels in the intestinal contents but not in plasma. As mentioned above, butyrate is an HDAC inhibitor; increased histone acetylation is generally associated with open chromatin and active transcription. Histone acetylation has also been shown to positively correlate with histone methylation *in vitro*[27], and the effects of histone methylation are more complex and depend upon both the site and degree of methylation. Additionally, histone post-translational modification (PTM) states are combinatorial and are thought to integrate cellular signals by sensing changes in the environment (namely via metabolite availability), ultimately mediating adaptive transcriptional responses[28].

We hypothesized that the effects of butyrate-producing bacteria on atherosclerosis may be mediated by changes that originate in the gut. To assess whether the presence of *R. intestinalis* impacted epigenetic programming in the colon or aorta in mice fed both diets, we surveyed >50 unique and combinatorial acetylated and methylated histone PTM states in proximal colon and aorta samples using a label-free data-independent acquisition mass spectrometry workflow (Supplementary Table 8)[29]. Principal components analysis of chromatin signatures reveals that *R. intestinalis* has a more pronounced effect on epigenetic programming in mice fed the HPP diet compared to animals fed the LPP diet (Supplementary Fig. 9). Although no changes were observed on histone H4, both acetylation and methylation of histone H3 and the variant histone H3.3, which is deposited in areas of active transcription, were affected by *R. intestinalis* (Fig. 3a-e). The majority of chromatin state changes induced by *R. intestinalis* in mice fed the HPP diet are indicative of active transcription. This includes increased abundance of highly methylated forms of K36 on histone H3 and H3.3 and the coeluting, isobaric peptides containing K18ac/K23ac, all of which are associated with activation of transcription or transcriptional elongation (Fig. 3b-d). These increases were accompanied by a significant decrease in peptides containing

Author Manuscript Author Manuscript Author Manuscript Author Manuscript

monomethylated and unmodified K36, suggesting a global shift toward more highly methylated forms of K36. Consistent with the very low colonization by *R. intestinalis*, these PTM states remained unchanged in the LPP-fed mice colonized with the "core plus *R. intestinalis*" community (Fig. 3b-d). Methylation of H3K4 and H3K79 is also associated with transcriptional activation. *R. intestinalis* induced an increase in K4me1 and K79me1, but a decrease in K4me3 and K79me2 in proximal colon of mice fed the HPP diet (Fig. 3a, e). Unexpectedly, there was a significant increase in K4me3 in response to *R. intestinalis* in mice fed the LPP diet (Fig. 3a). These data suggest that diet-microbiota interactions differentially regulate both histone methylation and acetylation in the intestine in response to *R. intestinalis*. In contrast, the presence of *R. intestinalis* did not elicit robust PTM changes in the aortas from mice fed both diets (Supplementary Fig. 10, Supplementary Table 9). Altogether, these results suggest that the presence of this butyrate-producing organism may alter susceptibility to atherosclerosis by affecting gene expression in the distal gut.

R. intestinalis regulates energy metabolism and reduces endotoxemia in mice fed the HPP diet.

To assess whether *R. intestinalis*–associated changes in colonic chromatin states affect gene expression, we performed RNA-seq analysis of colon tissues of HPP-fed mice. A total of 101 genes were differentially expressed (DE) between these two groups (FDR<0.05; Supplementary Table 10). Gene Ontology (GO) database terms for processes such as monocarboxylic acid metabolism, small molecule metabolism, and fatty acid metabolism were enriched among the genes that were significantly ($P < 0.05$) up-regulated in colons from "core plus *R. intestinalis*" mice compared to those from "core" controls (Fig. 4a). Specifically, there was a significant increase in the expression of genes associated with fatty acid oxidation such as *Acox1* (Acyl-CoA Oxidase 1), *Acsf2* (Acyl-CoA Synthetase Family Member 2), and *Decr2* (2,4-Dienoyl-CoA Reductase 2, peroxisomal). Conversely, GO terms associated with cellular response to glucose, hexose, and other monosaccharides, host immunity and inflammation such as leukocyte differentiation and TGFβ (transforming growth factor beta) receptor signaling pathway, were enriched among the genes downregulated in the colons from mice colonized with the "core plus *R. intestinalis*" community (Fig. 4b). Taken together, these results suggest that colonization with *R. intestinalis* switches the enterocyte energy substrate from glucose to butyrate, which is in agreement with a previous report showing that butyrate regulates energy metabolism in colonocytes[30].

Elegant studies have shown that the metabolic effects elicited by butyrate on intestinal epithelial cells enhance barrier function and decrease intestinal permeability[31]. Thus, we tested whether colonization with *R. intestinalis* impacted gut paracellular permeability *in vivo* using the fluorescein isothiocyanate (FITC)-dextran assay. We found that colonization with *R. intestinalis* decreased intestinal permeability, yet the difference did not reach significance (Fig. 4c), and resulted in significantly lower levels of plasma LPS (Fig. 4d). Consistent with this observation, we detected upregulation of tight junction genes such as *Cldn3* (Claudin3) and *Cldn4* in mice colonized with *R. intestinalis* (Supplementary Fig. 11, Supplementary Table 11). Collectively, our results suggest that *R. intestinalis* improves intestinal barrier function and reduces the amount of endotoxin in the bloodstream.

Author Manuscript Author Manuscript Author Manuscript Author Manuscript

Consistent with these findings, colonization with *R. intestinalis* resulted in a marked reduction of pro-inflammatory gene expression in the aorta (Fig. 2j). Furthermore, plasma levels of IL-12p40 was significantly decreased in mice colonized with *R. intestinalis* (Supplementary Fig. 12), which might be attributed to the reduction in aortic inflammatory molecules such as TNF-α and VCAM1 (Fig. 2j).

Butyrate has also been found to induce the differentiation of regulatory T cells (Tregs)[32], however, flow cytometric analysis detected no differences of $CD4^+$ T cells and Tregs in spleen or para-aortic lymph node samples between mice colonized with the two different communities (Supplementary Fig. 13a-c). We also investigated the effects of *R. intestinalis* gut colonization on T-cell/Treg-associated molecules and found no changes in the expression of *Cd4*, *Ifnγ* (Interferon γ), *Il-10*, and *Foxp3* (Forkhead box P3) in whole aorta (Supplementary Fig. 13c).

To further investigate whether *R. intestinalis* impacted circulating metabolites, we performed metabolome analysis of plasma using UPLC-MS/MS. A total of 678 metabolites were observed (Supplementary Fig. 14, Supplementary Table 12), 88 of which were differentially represented between the two groups of animals ($P<0.05$; for the purpose of generating hypotheses all metabolites showing a P value <0.05 were used for subsequent analyses). Enrichment analysis of differentially-represented metabolites showed that long chain fatty acid, phosphatidylethanolamine, eicosanoids, and branched chain amino acid metabolism were among the most regulated pathways (Supplementary Table 13). Levels of all 14 detected long chain fatty acids were lower in mice colonized with *R. intestinalis*, nine of which were significantly diminished ($P<0.05$; Fig. 4e, Supplementary Table 12). This is in line with previous work showing that butyrate upregulates oxidation of fatty acids in liver tissue. Alternatively, the reduction in long-chain fatty acids in mice colonized with *R. intestinalis* could be due to decreased lipolysis, which can be inhibited by butyrate[33].

Butyrate is known to upregulate ketogenesis in liver[34]. Consistent with this, the ketone body β-hydroxybutyrate was detected at higher levels in the "core plus *R. intestinalis*" colonized mice ($P=0.002$, $q<0.10$; Fig. 4e). β-hydroxybutyrate suppresses chronic inflammatory processes by inhibiting NLRP3 inflammasome-driven inflammatory responses[35]. There was also a reduction of all five eicosanoids detected in these mice; 12-hydroxyeicosatetraenoic acid (12-HETE) and 15-ketoeicosatetraenoic acid (15-KETE), which are 12/15-lipoxygenase products of arachidonic acid, were significantly lower ($P<0.05$, Fig. 4e, Supplementary Table 12). Interestingly, it has been shown that LPS induces inflammatory activation of arachidonic acid signaling in macrophages[36], which in turn promotes atherogenesis via production of IL-12[37] and/or oxidative modulation of low density lipoprotein[38]. Furthermore, we found significant positive correlations between eicosanoids and LPS levels in plasma (Supplementary Fig. 15). In summary, our data suggest that *R. intestinalis* stimulates fatty acid oxidation in enterocytes, improves endotoxemia, and results in the alteration of circulating eicosanoids, β-hydroxybutyrate, IL-12 and the amelioration of atherosclerosis.

Author Manuscript Author Manuscript Author Manuscript Author Manuscript

Tributyrin supplementation reduces the development of atherosclerotic plaque formation.

The data presented above suggest the athero-protective effect of *R. intestinalis* to be in part mediated by butyrate. In order to directly test this hypothesis, we conducted an experiment where tributyrin (TB), a triglyceride analogue of butyrate that is metabolized to butyrate by pancreatic lipases, was supplemented in the diet. Because there were three potential butyrate producers (*C. symbiosum*, *C. comes*, and *R. torques*) in the original "core" community, these bacteria were excluded and only confirmed non-butyrate producers (*Blautia hansenii*, *B. caccae*, *B. thetaiotaomicron*, *C. aerofaciens*, *Dorea longicatena*, *Marvinbryantii formatexigens*, and *P. stuartii*) were used as a "core II" community (Supplementary Table 14). Two groups of GF male *ApoE*$^{-/-}$ mice were orally gavaged with the "core II" community, and were fed the HPP diet or a 6% TB-supplemented diet (Fig. 5a). COPRO-Seq analysis showed that the TB treatment slightly increased the levels of *B. caccae* while it did not affect the abundance of other species in the community (Fig. 5b, Supplementary Table 15). As expected dietary TB supplementation resulted in a significant increase of cecal butyrate levels, although these were relatively low (~ 0.1μmoles/g wt), suggesting that most of butyrate derived from TB might be absorbed in the distal small intestine (Supplementary Fig. 16a). Supplementation of TB did not impact acetate or propionate levels in the cecum (Supplementary Fig. 16a) nor SCFAs in plasma (Supplementary Fig. 16b). Importantly, we found that administration of TB significantly inhibited the development of atherosclerosis (Fig. 5c, e), lipid deposition (Fig. 5c, f), and macrophage accumulation (Fig. 5d, g) in the plaque while it did not change the levels of plasma lipid profile (Supplementary Table 6), collagen (Supplementary Fig. 17a, c) or smooth muscle cells (Supplementary Fig. 17b, d) in the aortic sinus. Consistent with the results observed with *R. intestinalis*, TB supplementation did not affect levels of $CD4^+$ T cells and Tregs in spleen or para-aortic lymph node samples (Supplementary Fig. 18). Moreover, TB supplementation significantly reduced gut permeability as measured by the FITC-dextran assay as well as plasma LPS levels (Fig. 5h, i). These results suggest that butyrate inhibits the development of atherosclerosis at least in part by reducing endotoxemia and that butyrate mediates the vascular benefits associated with increased *Roseburia* colonization.

Discussion

A large body of literature supports the notion that consumption of dietary fiber decreases the risk of cardiometabolic disease[39]. Recent studies suggest that some of the benefits associated with consumption of dietary fiber are mediated in part by gut microbes[40], with increased representation of butyrate-producing microbes proposed as one of the potential mediators[41]. Moreover, butyrate producers have been frequently found at higher levels in healthy populations relative to patients suffering various inflammatory and metabolic diseases[16,18,19]. Our study provides causal evidence linking increased abundance of butyrate-producing bacteria with: (i) higher cecal levels of butyrate; (ii) epigenetic, transcriptional and metabolic changes in the intestine; (iii) decreased systemic markers of inflammation; and (iv) smaller atherosclerotic lesions.

Previous work revealed that butyrate regulates generation of colonic Tregs through histone deacetylase inhibition, and Tregs have been shown to inhibit atherosclerosis by dampening

Author Manuscript Author Manuscript Author Manuscript Author Manuscript

effector T cell responses[32,42], however, we did not observe any significant difference of Tregs in the aorta or in paraaortic lymph nodes, suggesting that, at least in our studies, the observed athero-protective effect seems to be independent of aortic Treg cells. The effects of butyrate-producing bacteria on atherosclerosis and inflammation could be linked to the metabolic effects that butyrate has in the intestine. Butyrate is efficiently absorbed and oxidized to acetyl-CoA in mitochondria, and represents the main fuel for normal colonocytes. We found that introduction of *R. intestinalis* alters histone epigenetic states and modulates gene expression in the gut. The observed changes in gene expression suggest that the presence of the butyrate-producer directed epithelial metabolism away from glycolysis and toward fatty acid utilization. Butyrate oxidation increases epithelial O_2 consumption and stabilization of hypoxia-inducible factor (HIF)[43], which in turn can enhance epithelial barrier function *in vitro* and *in vivo*[44]. This is consistent with our findings that the expression of several genes in mitochondrial fatty acid oxidation was significantly upregulated. While we did not observe evidence of transcriptionally regulated genes downstream of HIF, we cannot exclude possible involvement of this pathway. Butyrate can reach the liver via portal circulation, where it also stimulates β-oxidation and ketogenesis[34]. Untargeted mass spectrometry suggested that *R. intestinalis*-dependent increase in butyrate stimulates oxidation of long-chain fatty acids and production of ketone bodies. The increase on the ketone body β-hydroxybutyrate may contribute to the protective effect of *R. intestinalis*, as this metabolite has been shown to inhibit key inflammatory pathways involved in atherosclerosis.

An additional mechanism by which *R. intestinalis* impacts the host relates to the effects of butyrate on chromatin, as butyrate is a HDAC inhibitor[45]. However, the presence of *R. intestinalis* and a dramatic increase in butyrate levels did not result in extensive changes of colonic histone acetylation, apart from a modest increase in H3K18/K23 acetylation. In contrast, we observed larger effects on histone methylation that predict an active chromatin state. Given the combinatorial nature of histone modifications, it is possible that HDAC inhibition can also impact histone methylation. Indeed, methylation of H3K4 has been shown to preferentially occur on acetylated histones in cultured cells treated with HDAC inhibitors[27]. Collectively, our findings suggests that *R. intestinalis* affects host histone methylation as well as acetylation, impacting gene expression in the colon. Although understanding the impact of these changes upon histone PTM will require further analysis, we speculate that these observations may provide a mechanistic link between changes in nutrient availability (i.e., butyrate) and the effects in gene expression related to energy metabolism caused by the introduction of the prominent butyrate-producer.

In summary, we show that colonization with *R. intestinalis* lowers endotoxemia, possibly by improving barrier function, reduces inflammatory markers in plasma and aorta, and the extent of atherosclerotic lesion in a diet-dependent fashion. Our results suggest that athero-protective effect of *R. intestinalis* is mediated at least in part by butyrate. Additionally, *R. intestinalis* may impact the host via different molecules through mechanisms not examined in this study. Future experiments using GF mice colonized with defined communities with different abundances of butyrate producers supplied with different types of dietary polysaccharides will inform synbiotic approaches for prevention and/or treatment of cardiovascular disease.

Author Manuscript Author Manuscript Author Manuscript Author Manuscript

Methods

The Ath-HMDP studies.

The animal work of the Ath-HMDP panel was conducted as previously described[22]. Briefly, mice carrying the human transgene for CETP in a C57BL/6 background were obtained from The Jackson Laboratory (Stock Number:003904). Mice carrying the human ApoE3 Leiden variant were kindly provided by Dr. L. Havekes. For purposes of these experiments, we interbred these mice to create a strain carrying both transgenes and these were bred to females from ~100 common inbred and recombinant inbred strains purchased from The Jackson Laboratory. Male and female progeny were genotyped for the presence of both transgenes and, at the age of about 8 weeks, were placed on a “Western Style” synthetic high fat diet (33 kcal % fat from cocoa butter) supplemented with 1% cholesterol (Research Diets D10042101, Supplementary Table 16). Mice from different strains and sex were housed in separate cages, but in the same room throughout the study. After 16 weeks on this diet, 147 male and 195 female mice (83 strains in total) were euthanized for collection of tissue. Euthanasia of mice was carried out using deep anesthesia with isoflurane vapor followed by cervical dislocation. The animal work of the Ath-HMDP panel was conducted according to relevant national and international guidelines and was approved by the UCLA Animal Research Committee, the UCLA IACUC.

Sequencing of 16S rRNA genes.

Ceca from a total of 195 female mice (71 strains) and 147 male mice (60 strains) were profiled for bacterial taxa using 16S rRNA gene sequencing. Microbial DNA was extracted using the PowerSoil DNA Isolation Kit (MO BIO Laboratories, Carlsbad, CA). Amplification and sequencing of V4 hypervariable region of the 16S rRNA gene was performed using the validated, region-specific bacterial primers 515F and 806R. The reverse amplification primer contained a 12-bp Golay error-correcting barcode sequence and amplicons were generated in triplicate using 5 Prime Hot MasterMix (Fischer Scientific, UK). The PCR conditions consisted of an initial denaturation step of 94°C for 3 min; 35 cycles of 94°C for 45 sec, 50°C for 30 sec, and 72°C for 90 sec., followed by 72°C for 5 min. Replicate amplicons were quantified with Quanti-iT™PicoGreen dsDNA Assay Kit (Life Technologies Corporation, Carlsbad, CA), pooled (200ng from 96 samples) and purified using with the UltraClean PCR Clean-up Kit (MOBIO Laboratories, Inc., Carlsbad, CA). The purified, pooled PCR products were sequenced on a 454 pyrosequencing platform according to the Roche 454 recommended procedures. De-multiplexing 16S rRNA gene sequences, quality control and operational taxonomic unit (OTU) binning were performed using the open source pipeline Quantitative Insights Into Microbial Ecology (QIIME) version 1.7.0. Quality-filtered reads were de-multiplexed, yielding an average length of 298 bases per read, and an average coverage of 2510 sequences per sample. Sequences were binned into OTUs based on 97% identity using UCLUST against the Greengenes reference database. Each sample’s sequences were rarefied to a depth of 200 reads to reduce the effect of sequencing depth. Microbial composition at each taxonomic level was defined using the summarize_taxa function in QIIME. The relative abundance of each taxon was calculated by dividing the sequences pertaining to a specific taxon by the total number of bacterial sequences for that sample.

Author Manuscript Author Manuscript Author Manuscript Author Manuscript

Correlation analysis.

The biweight midcorrelation statistic is analogous to the Pearson correlation coefficient, but has the advantage of being robust to outliers. We used the bicor function implemented in the WGCNA R package to calculate the microbiota-lesion size correlations in the Ath-HMDP panel.

Growth medium.

All bacteria were grown on Mega Medium (Supplementary Table 17). This medium was filter sterilized and stored in a Coy anaerobic chamber (5% H_2, 20% CO_2, and 75% N_2)[46].

Gnotobiotic husbandry.

All experiments involving gnotobiotic mice were performed using protocols approved by the University of Wisconsin-Madison Animal Care and Use Committee. All GF C57BL/6 *ApoE* $^{-/-}$ mice were maintained in a controlled environment in plastic flexible film gnotobiotic isolators under a strict 12h light/dark cycle and received sterilized water and standard chow (LabDiet 5021; LabDiet, St Louis, MO) *ad libitum* until 8 weeks of age. Sterility of GF animals was assessed by incubating freshly collected fecal samples under aerobic and anaerobic conditions using standard microbiology methods.

Gnotobiotic mouse colonization.

Aliquots of each frozen bacterial strain were inoculated into 10 mL of Mega Medium and grow anaerobically at 37°C overnight. Strains belonging to the same community were then combined in an equal volume ratio in a sterile and anaerobic Hungate tube. In the experiments shown Fig. 1a and Supplementary Fig. 6a, 8-week-old GF male mice were inoculated by oral gavage with 0.2 mL of mixed bacterial culture, “core” community or “core plus *R. intestinalis*” (Supplementary Table 3), in the gnotobiotic isolator. Mice were switched to a standard grain-based chow diet (Supplementary Table 18, TD.2918; Envigo, Madison, WI) or a purified diet composed of 19.3% (w/w) protein, 64.8% carbohydrate, and 5.1% fat (Supplementary Table 19, TD.00278; Envigo). Dietary fiber in the chow diet is derived from a variety of plants including ground wheat, ground corn, wheat middlings, dehulled soybean meal, and corn gluten meal (Supplementary Table 20). Experimental diets were sterilized by irradiation. Mice were then euthanized at 26 weeks of age after 4h fasting. In the experiment shown in Fig. 5a, 6-week-old GF male mice were inoculated by oral gavage with 0.2 mL of mixed bacterial culture “core II” (Supplementary Table 14) in the gnotobiotic isolator. Mice were switched to a control chow diet (Supplementary Table 18, TD.2918) or a 6% tributyrin-supplemented chow diet. The mice were then euthanized at 22 weeks of age after 4h fasting.

A statement about the experimental design.

Power and sample size: we determined the mean sample variance in atherosclerosis lesion size (μm^2) using data from our preliminary studies in gnotobiotic *ApoE* KO mice and found that using a minimum of 8 mice per group is necessary to detect atherosclerotic lesion changes of 20% or greater, assuming α=0.05 and power=0.80. Replication: in atherosclerosis experiments shown in Fig. 2, Fig. 5, and Supplementary Fig. 6, we

Author Manuscript Author Manuscript Author Manuscript Author Manuscript

performed two sets of experiments using animals from different litters, and combined results in the figures. No randomization protocols or blinded analysis were employed.

Atherosclerotic lesion assessments.

Atherosclerotic lesions were assessed as previously described[12]. Briefly, mice were anesthetized and the aorta was perfused with PBS. To assess the atherosclerotic lesion size at the aortic sinus, the samples were cut in the ascending aorta, and the proximal samples containing the aortic sinus were embedded in OCT compounds (Tissue-Tek; Sakura Finetek, Tokyo, Japan). Five consecutive sections (10 μm thickness) taken at 100 μm intervals (i.e. 50, 150, 250, 350, and 450 μm from the bottom of the aortic sinus) were collected from each mouse and stained with Oil Red O. Plaque area and Oil Red O-positive area were measured using Image J software (National Institutes of Health, Bethesda, MD). The volume of atherosclerosis in the aortic sinus was expressed as mean size of the 5 sections for each mouse. Immunohistochemistry was performed on formalin-fixed cryosections of mouse aortic roots using antibodies to identify macrophages (MOMA-2, 1:50; ab33451, Abcam, Cambridge, MA), followed by detection with biotinylated secondary antibodies (1:400; ab6733, Abcam) and streptavidin-horseradish peroxidase (1:500; P0397, Dako, Carpinteria, CA). Smooth muscle cells were identified by immunostaining with fluorescein isothiocyanate (FITC)-conjugated primary antibody against α-smooth muscle actin (1:100; clone 1A4, Sigma), followed by anti-FITC biotin-conjugated secondary antibody (1:400; clone FL-D6, Sigma). Negative controls were prepared with substitution with an isotype control antibody. Staining with Masson's trichrome was used to delineate the fibrous area according to the manufacturer's instructions (ab150686, Abcam). Stained sections were digitally captured, and the percentage of the stained area (the stained area per total atherosclerotic lesion area) was calculated.

COPRO-Seq analysis.

Bacterial communities resulting from inoculation of GF animals were analyzed using Illumina sequencing according to the COPRO-Seq (*co*mmunity *pro*filing by *seq*uencing) method[47]. Feces were collected 4 weeks after the colonization. In short, DNA isolated from feces via bead beating was used to prepare libraries for shotgun Illumina sequencing. Five hundred nanograms of DNA from each sample was fragmented by sonication and subjected to enzymatic blunting and adenine tailing. Customized Illumina adapters containing maximally distant 8-bp bar codes were ligated to the poly (A)-tailed DNA. Gel-extracted DNA (size selection ~250 to 300bp) was amplified by PCR using primers and cycling conditions recommended by Illumina. Purified PCR products were submitted to the UW-Madison Biotechnology Center for a single end 50-bp Illumina MiSeq run. Results were processed using the software pipeline detailed by McNulty *et al*[47].

Plasma biochemical analysis.

Blood samples were drawn by cardiac puncture under anesthesia using isoflurane. Plasma was acquired by centrifugation and stored at −80°C until measurement. The levels of triglycerides, total cholesterol, and high-density lipoprotein cholesterol were measured with commercially available kits from Wako Chemicals (Richmond, VA). Quantification of plasma cytokines was carried out using the Bio-plex 23 cytokine mouse array (Bio-Rad,

Author Manuscript Author Manuscript Author Manuscript Author Manuscript

Hercules, CA) as per manufacturer's instructions. Cytokines profiled were: Eotaxin, G-CSF, GM-CSF, IFN-γ, IL-1α, IL-1β, IL-2, IL-3, IL-4, IL-5, IL-6, IL-9, IL-10, IL-12 (p40), IL-12 (p70), IL-13, IL-17A, KC, MCP-1, MIP-1α, MIP-1β, RANTES, TNF-α. Plasma lipopolysaccharide (LPS) levels were quantitated with the QCL-1000 Endpoint Chromogenic LAL Assay (Lonza, Basel, Switzerland). Intestinal permeability was assessed using the non-metabolizable macromolecule Fluorescein Isothiocyanate (FITC)-Dextran (4kDA, Sigma). Mice were fasted overnight and gavaged with FITC-dextran (44mg/100g body weight) 4 hours before bleeding. The concentration of FITC-dextran in serum was quantified spectrophotofluorometrically.

GC-MS of short chain fatty acid measurement.

Sample preparation was based on a previously described procedure[48] with some modifications. Cecal contents were weighed in 4mL vials, then 10 μL of a mixture of internal standards (20 mM each; acetic acid-D4, Sigma-Aldrich #233315; propionic acid-D6, Sigma-Aldrich #490644; and butyric acid-D7, CDN isotopes #D-171) was subsequently added, followed by 20 μL of 33% HCl and 1 mL diethyl ether and the vials were sealed with polytetrafluoroethylene-lined screw caps. For plasma samples, 50 μL of each sample, 1.25 μL of the internal standard mix, 5 μL of 33% HCl, and 0.75 mL of diethyl ether were mixed. The mixture was vortexed vigorously for 3 min and then centrifuged (4,000 x *g*, 10 min). The upper organic layer was transferred to another vial and a second diethyl ether extraction was performed. After combining the two ether extracts, a 60 μL aliquot was removed, combined with 2 μL *N*-*tert*-butyldimethylsilyl-*N*-methyltrifluoroacetamide (MTBSTFA, Sigma-Aldrich #394882) in a GC auto-sampler vial with a 200 μL glass insert, and incubated for 2 h at room temperature. Derivatized samples (1 μL) were injected onto an Agilent 7890B/5977A GC/MSD instrument with Agilent DB1-ms 0.25 mm x 60 m column with 0.25 μm bonded phase. A discontinuous oven program was used stating at 40°C for 2.25 min, then ramping at 20°C/min to 200°C, then ramping at 100°C/min to 300°C and holding for 7 min. The total run time was 18.25 minutes. Linear column flow was maintained at 1.26mL/min. The inlet temperature was set to 250°C with an injection split ratio of 15:1. Quantitation was performed using selected ion monitoring (SIM) acquisition mode and metabolites were compared to relevant labeled internal standards using Agilent Mass Hunter v. Acquisition B.07.02.1938. The m/z of monitored ions are as follows: 117 (acetic acid), 120 (acetic acid-D4), 131 (propionic acid), 136 (propionic acid-D6), 145 (butyric acid), and 151 (butyric acid-D7). Concentrations were normalized to mg of cecal contents.

Untargeted metabolome for plasma samples.

Untargeted mass spectrometry data were collected at Metabolon Inc (Durham, NC). Plasma samples were prepared using the automated MicroLab STAR system (Hamilton Company, Bonaduz, Switzerland). To remove protein, dissociate small molecules bound to protein or trapped in the precipitated protein matrix, and to recover chemically diverse metabolites, proteins were precipitated with methanol under vigorous shaking for 2 min (Glen Mills GenoGrinder 2000) followed by centrifugation. The resulting extract was divided into five fractions: two for analysis by two separate reverse phase (RP)/UPLC-MS/MS methods with positive ion mode electrospray ionization (ESI), one for analysis by RP/UPLC-MS/MS with

Author Manuscript Author Manuscript Author Manuscript Author Manuscript

negative ion mode ESI, one for analysis by HILIC/UPLC-MS/MS with negative ion mode ESI, and one sample was reserved for backup. Samples were placed briefly on a TurboVap (Zymark) to remove the organic solvent. The sample extracts were stored overnight under nitrogen before preparation for analysis.

Ultrahigh Performance Liquid Chromatography-Tandem Mass Spectroscopy (UPLC-MS/MS).—All methods utilized a Waters ACQUITY ultra-performance liquid chromatography (UPLC) and a Thermo Scientific Q-Exactive high resolution/accurate mass spectrometer interfaced with a heated electrospray ionization (HESI-II) source and Orbitrap mass analyzer operated at 35,000 mass resolution. The sample extract was dried then reconstituted in solvents compatible to each of the four methods. Each reconstitution solvent contained a series of standards at fixed concentrations to ensure injection and chromatographic consistency. One aliquot was analyzed using acidic positive ion conditions, chromatographically optimized for more hydrophilic compounds. In this method, the extract was gradient eluted from a C18 column (Waters UPLC BEH C18–2.1×100 mm, 1.7 μm) using water and methanol, containing 0.05% perfluoropentanoic acid (PFPA) and 0.1% formic acid (FA). Another aliquot was also analyzed using acidic positive ion conditions, however it was chromatographically optimized for more hydrophobic compounds. In this method, the extract was gradient eluted from the same aforementioned C18 column using methanol, acetonitrile, water, 0.05% PFPA and 0.01% FA and was operated at an overall higher organic content. Another aliquot was analyzed using basic negative ion optimized conditions using a separate dedicated C18 column. The basic extracts were gradient eluted from the column using methanol and water, amended with 6.5mM ammonium bicarbonate at pH 8. The fourth aliquot was analyzed via negative ionization following elution from a HILIC column (Waters UPLC BEH Amide 2.1×150 mm, 1.7 μm) using a gradient consisting of water and acetonitrile with 10mM ammonium formate, pH 10.8. Compounds were identified by comparison to library entries based upon retention time/index, mass to charge ratio (m/z) and chromatographic data, and peaks were quantified using area-under-the curve.

Statistical analysis.—The dataset comprises a total of 678 compounds of biochemicals. Metabolic profiles were quantified in terms of relative abundance and median scaled to 1. Following log transformation and imputation of missing values, if any, with the minimum observed value for each compound, Welch's two-sample *t*-test was used to identify biochemicals that differed significantly between experimental groups. An estimate of the false discovery rate (*q*-value) is calculated to take into account the multiple comparisons that normally occur in metabolomic-based studies. Enrichment pathways were determined by completing pathway set enrichment analysis within MetaboLync pathway analysis software. For this analysis all metabolites with P value < 0.05 were included. For individual pair-wise comparison, pathway enrichment displays the number of experimentally regulated compounds relative to all detected compounds in a pathway, compared to the total number of experimentally regulated compounds relative to all detected compounds in the study (Supplementary Table 13).

Author Manuscript Author Manuscript Author Manuscript Author Manuscript

Histone post-translation modification (PTM) quantification with mass spectrometry:

Tissue fraction, histone extraction, and label-free chemical derivatization.— Nuclear fractions were prepared from flash-frozen whole post-mortem colon and aorta tissues. In brief, 50 mg of tissue was homogenized on ice in hypotonic lysis buffer (10mM Tris-HCl, 10mM NaCl, and 3mM $MgCl_2$) with histone deacetylase and protease inhibitors (1mM sodium butyrate, 4 μM trichostatin A, 100 μM phenylmethylsulfonyl fluoride, 10 μg/mL leupeptin, and 10 μg/mL aprotinin). Crude sub-cellular fractions were separated by differential centrifugation at 800 x g for 10 minutes at 4°C. The crude nuclear pellet was then washed twice with ice-cold PBS prior to acid extraction. Histones were acid extracted as described previously[49]. Histone extract (5 μg) was then subjected to a hybrid chemical derivatization method using propionic anhydride to label protein N-termini and all unmodified and monomethylated lysine residues, followed by trypsinization for 6 hours at 37°C, and derivatization of newly generated peptide N-termini with phenylisocyanate. This chemical derivatization method protects all lysine residues from cleavage by trypsin, which cleaves C-terminally to unmodified lysine and arginine residues, enabling consistent generation of histone peptides amenable to analysis by mass spectrometry. Derivatized histone extracts were then desalted using in-house C18 stage tips.

Nano-liquid chromatography and electrospray ionization tandem mass spectrometry.—For each sample, 0.3 μg of derivatized histone peptides was injected onto a Dionex Ultimate3000 nanoflow HPLC with a Waters nanoAcquity UPLC C18 column (100 m x 150 mm, 3m) online with a Thermo Fisher Q-Exactive mass spectrometer eluted at 700 nL/min. Mobile phase consisted of water + 0.1% formic acid (A) and acetonitrile + 0.1% formic acid (B). Histone peptides were resolved with a 2-step linear gradient of 2% to 25% mobile phase B over 60 minutes followed by 25% to 40% mobile phase B over 15 minutes. Data was acquired using data-independent acquisition (DIA) mode. The mass spectrometer was operated with an MS1 scan at resolution = 35,000, automatic gain control target = 1×10^6, and scan range = 390–910 m/z, followed by a DIA scan with a loop count of 10. DIA settings were as follows: window size = 10 m/z, resolution = 17,500, automatic gain control target = 1×10^6, DIA maximum fill time = AUTO, and normalized collision energy = 30. For each cycle, one full MS1 scan was followed by 10 MS2 scans using an isolation window size of 10 m/z.

Histone post-translation modification (PTM) quantification.—The Thermo.raw files were imported into Skyline for quantitative analysis as previously described[49]. Briefly, all MS1 and MS2 peaks were matched to an in-house spectral library upon import based on retention times and the presence of appropriate transitions. All imported histone peptide MS1 peaks and their integration bounds were also manually verified using XCalibur Qual Browser (v2.2). Peak areas for all selected transitions were exported and precursor ion peak areas were combined for quantitation. Exported peak area values from Skyline were normalized within peptide families to the total area prior to calculation of fold changes and statistics. All p-values were generated using a Welch's t-test. Statistical significance was determined by $P < 0.05$.

Author Manuscript Author Manuscript Author Manuscript Author Manuscript

RNA-seq analysis.

RNA was extracted from frozen livers by TRIzol extraction and then further cleaned using the Qiagen RNeasy Mini Kit and quantified using a Nanodrop 2000 spectrophotometer. A single-end cDNA library was prepared using the Illumina TruSeq stranded mRNA Sample Preparation kit (RS-122–2101) according to the manufacturer's specifications. Samples were multiplexed, normalized, and pooled prior to sequencing on a HiSeq2500 at the University of Wisconsin-Madison Biotechnology Center. Sequencing reads were processed and filtered using the FastX Toolkit. The first 10 bp of each read were removed to eliminate GC bias at the beginning of each read using the FastX Trimmer. The 6-bp Illumina adapter sequences were then clipped using the FastX Clipper and a quality filter was applied to all reads to eliminate any reads with a quality score <30 as determined by the FastX Quality Filter. Reads were then aligned to the mm9 mouse reference genome constructed to include only annotated genes (NM_RefSeqs) by Bowtie2 alignment. Seed length was set to 28 and allowed 2 mismatches per seed. Gene expression was then calculated using RSEM with a forward probability of 0.0 (for stranded libraries). Differential expression (DE) was calculated using EBSeq with a false discovery rate (FDR) = 0.05. DE genes were curated by hand for functional clustering analysis.

Quantitative Real-Time PCR.

Total RNA was extracted from whole aorta with TRizol reagent (Invitrogen, Carlsbad, CA). SuperScript II Reverse Transcriptase with oligo (dT) primer (all from Invitrogen) was used to synthesize 20μl cDNA templates from 100ng purified RNA. cDNA was diluted 2X before use and qRT-PCR reactions were prepared in a 10μl volume using SsoAdvanced Universal SYBR Green Supermix (Bio-Rad) and 400nM specific primers targeting the gene of interest. Reactions were run on a CFX96 Real-Time PCR System (Bio-Rad). The primer sequences for amplification of each transcript are listed in Supplementary Table 21. Relative gene expression was calculated by the ΔΔCt method using β-actin as an internal control.

Flow cytometric analysis.

For analyses of immune cells by flow cytometry, splenocytes and paraaortic lymph node cells were isolated and stained in PBS containing 2% fetal calf serum. Flow cytometry analysis was performed using BD LSRFortessa (BD Biosciences, San Jose, CA) or Attune NxT Flow Cytometer (Thermo Fisher Scientific, Waltham, MA) with FlowJo software (Tree Star, Ashland, OR). The antibodies used were as follows; anti-TCRβ (clone H57–597; Biolegend, San Diego, CA), anti-CD4 (cloneRM4–5; Biolegend), anti-Foxp3 (clone FJK-16s; eBioscience). Intracellular staining of Foxp3 was performed using the Foxp3 staining buffer set (eBioscience) according to the manufacturer's instructions. The fluorescent staining was performed after blocking the Fc receptor with the anti-CD16/CD32 antibody. Surface staining was performed according to standard procedures at a density of 1×10^6 cells per 50 μL, and the volumes were scaled up accordingly.

Statistical Analysis.

The data were expressed as individual dots with mean ± SEM or box-and whisker plots where the center line was the median, boxes extend to 25th and 75th percentiles, and whisker

Author Manuscript Author Manuscript Author Manuscript Author Manuscript

extend to min and max values, and analyzed using GraphPad Prism 6.0 (GraphPad Software) or R (3.4.1). Significant differences between two groups were evaluated by two-tailed unpaired Student's *t* tests or two-tailed Welch's T-test. In multiple testing, FDRs were computed using the Benjamini-Hochberg procedure. The level of significance was set at P value < 0.05 or FDR value < 0.10. The statistical analysis for RNA-seq and untargeted metabolome analyses were described in each Method section.

Reporting summary.

Further information on experimental design is available in the Nature Research Reporting Summary linked to this paper.

Data availability.

The SRA accession ID for COPRO-Seq is SRP158926. The accession number for RNA sequencing data is GEO: GSE119141. The SRA accession ID for the Ath-HMDP microbiome data is SRP142550. Additional data that support the findings of this study are available from the corresponding author upon reasonable request.

Supplementary Material

Refer to Web version on PubMed Central for supplementary material.

Acknowledgments

The authors would like to thank C. Pan (UCLA) for help in 16S sequencing, G.A. Barrett-Wilt (University of Wisconsin Mass Spectrometry Facility) for technical support with GC/MS analysis, D.A. Roenneburg (Department of Surgery, University of Wisconsin School of Medicine and Public Health) for assistance with histology, and B.D. Mickelson (Envigo) for assistance with diets. We also thank the University of Wisconsin Biotechnology Center DNA Sequencing Facility for providing sequencing and support services. This work was supported in part by grants NIH DK108259 (to F.E.R.) and HL30568 (to A.J.L.), by the National Institute of Food and Agriculture, U.S. Department of Agriculture, under award number 2016–67017-24416 (to F.E.R.) and the Swedish Heart Lung Foundation (to F.B.). This work was also supported in part by a grant from a Transatlantic Networks of Excellence Award 17CVD01 from Foundation Leducq. K.K. is supported by Astellas Foundation for Research on Metabolic Disorders, International Atherosclerosis Society, Yamada Science Foundation, and Sumitomo Life Welfare and Culture Foundation. K.A.K. is supported by NIH F30 DK108494–02.

References

1. Kau AL, Ahern PP, Griffin NW, Goodman AL & Gordon JI Human nutrition, the gut microbiome and the immune system. Nature 474, 327–336 (2011). [PubMed: 21677749]
2. Hooper LV, Midtvedt T & Gordon JI How host-microbial interactions shape the nutrient environment of the mammalian intestine. Annu. Rev. Nutr. 22, 283–307 (2002). [PubMed: 12055347]
3. Xu J et al. Evolution of Symbiotic Bacteria in the Distal Human Intestine. PLoS Biol. 5, e156 (2007). [PubMed: 17579514]
4. Martens EC, Koropatkin NM, Smith TJ & Gordon JI Complex glycan catabolism by the human gut microbiota: The bacteroidetes sus-like paradigm. J. Biol. Chem. 284, 24673–24677 (2009). [PubMed: 19553672]
5. Koropatkin NM, Cameron EA & Martens EC How glycan metabolism shapes the human gut microbiota. Nat. Rev. Microbiol. 10, 323–335 (2012). [PubMed: 22491358]
6. Martens EC, Kelly AG, Tauzin AS & Brumer H The devil lies in the details: How variations in polysaccharide fine-structure impact the physiology and evolution of gut microbes. J. Mol. Biol. 426, 3851–3865 (2014). [PubMed: 25026064]

Author Manuscript Author Manuscript Author Manuscript Author Manuscript

7. Schnorr S et al. Gut microbiome of the Hadza hunter-gatherers. Nat. Commun. 5, 3654 (2014). [PubMed: 24736369]
8. Sonnenburg ED et al. Diet-induced extinctions in the gut microbiota compound over generations. Nature 529, 212–215 (2016). [PubMed: 26762459]
9. Ritzhaupt A, Ellis A, Hosie KB & Shirazi-Beechey SP The characterization of butyrate transport across pig and human colonic luminal membrane. J. Physiol. 507, 819–830 (1998). [PubMed: 9508842]
10. Candido EPM, Reeves R & Davie JR Sodium butyrate inhibits histone deacetylation in cultured cells. Cell 14, 105–113 (1978). [PubMed: 667927]
11. Segain JP et al. Butyrate inhibits inflammatory responses through NFkappaB inhibition: implications for Crohn's disease. Gut 47, 397–403 (2000). [PubMed: 10940278]
12. Kasahara K et al. Commensal bacteria at the crossroad between cholesterol homeostasis and chronic inflammation in atherosclerosis. J. Lipid Res. 58, 519–528 (2017). [PubMed: 28130274]
13. Mitchell JA, Ryffel B, Quesniaux VFJ, Cartwright N & Paul-Clark M Role of pattern-recognition receptors in cardiovascular health and disease. Biochem. Soc. Trans. 35, 1449–1452 (2007). [PubMed: 18031243]
14. Wang Z et al. Gut flora metabolism of phosphatidylcholine promotes cardiovascular disease. Nature 472, 57–65 (2011). [PubMed: 21475195]
15. Tang WHW et al. Intestinal Microbial Metabolism of Phosphatidylcholine and Cardiovascular Risk. N. Engl. J. Med. 368, 1575–1584 (2013). [PubMed: 23614584]
16. Karlsson FH et al. Symptomatic atherosclerosis is associated with an altered gut metagenome. Nat. Commun. 3, 1245 (2012). [PubMed: 23212374]
17. Louis P, Young P, Holtrop G & Flint HJ Diversity of human colonic butyrate-producing bacteria revealed by analysis of the butyryl-CoA:acetate CoA-transferase gene. Environ. Microbiol. 12, 304–314 (2010). [PubMed: 19807780]
18. Qin J et al. A metagenome-wide association study of gut microbiota in type 2 diabetes. Nature 490, 55–60 (2012). [PubMed: 23023125]
19. Karlsson FH et al. Gut metagenome in European women with normal, impaired and diabetic glucose control. Nature 498, 99–103 (2013). [PubMed: 23719380]
20. Walker AW et al. Dominant and diet-responsive groups of bacteria within the human colonic microbiota. ISME J. 5, 220–230 (2011). [PubMed: 20686513]
21. Duncan SH et al. Reduced dietary intake of carbohydrates by obese subjects results in decreased concentrations of butyrate and butyrate-producing bacteria in feces. Appl. Environ. Microbiol. 73, 1073–1078 (2007). [PubMed: 17189447]
22. Bennett BJ et al. Genetic Architecture of Atherosclerosis in Mice: A Systems Genetics Analysis of Common Inbred Strains. PLoS Genet. 11, e1005711 (2015). [PubMed: 26694027]
23. Duncan SH, Barcenilla A, Stewart CS, Pryde SE & Flint HJ Acetate utilization and butyryl coenzyme A (CoA):acetate-CoA transferase in butyrate-producing bacteria from the human large intestine. Appl. Environ. Microbiol. 68, 5186–5190 (2002). [PubMed: 12324374]
24. Guilloteau P et al. From the gut to the peripheral tissues: The multiple effects of butyrate. Nutr. Res. Rev. 23, 366–384 (2010). [PubMed: 20937167]
25. Cybulsky MI et al. A major role for VCAM-1, but not ICAM-1, in early atherosclerosis. J. Clin. Invest. 107, 1255–1262 (2001). [PubMed: 11375415]
26. Boesten LSM et al. Tumor necrosis factor-α promotes atherosclerotic lesion progression in APOE*3-leiden transgenic mice. Cardiovasc. Res. 66, 179–185 (2005). [PubMed: 15769461]
27. Nightingale KP et al. Cross-talk between histone modifications in response to histone deacetylase inhibitors: MLL4 links histone H3 acetylation and histone H3K4 methylation. J. Biol. Chem. 282, 4408–4416 (2007). [PubMed: 17166833]
28. Fan J, Krautkramer KA, Feldman JL & Denu JM Metabolic regulation of histone post-translational modifications. ACS Chem. Biol. 10, 95–108 (2015). [PubMed: 25562692]
29. Krautkramer KA, Reiter L, Denu JM & Dowell JA Quantification of SAHA-Dependent Changes in Histone Modifications Using Data-Independent Acquisition Mass Spectrometry. J. Proteome Res. 14, 3252–3262 (2015). [PubMed: 26120868]

Author Manuscript Author Manuscript Author Manuscript Author Manuscript

30. Donohoe DR et al. The microbiome and butyrate regulate energy metabolism and autophagy in the mammalian colon. Cell Metab. 13, 517–526 (2011). [PubMed: 21531334]
31. Peng L, Li Z-R, Green RS, Holzman IR & Lin J Butyrate Enhances the Intestinal Barrier by Facilitating Tight Junction Assembly via Activation of AMP-Activated Protein Kinase in Caco-2 Cell Monolayers. J. Nutr. 139, 1619–1625 (2009). [PubMed: 19625695]
32. Furusawa Y et al. Commensal microbe-derived butyrate induces the differentiation of colonic regulatory T cells. Nature 504, 446–450 (2013). [PubMed: 24226770]
33. Ohira H et al. Butyrate attenuates inflammation and lipolysis generated by the interaction of adipocytes and macrophages. J. Atheroscler. Thromb. 20, 425–42 (2013). [PubMed: 23470566]
34. Li H et al. Sodium butyrate stimulates expression of fibroblast growth factor 21 in liver by inhibition of histone deacetylase 3. Diabetes 61, 797–806 (2012). [PubMed: 22338096]
35. Youm YH et al. The ketone metabolite β-hydroxybutyrate blocks NLRP3 inflammasome-mediated inflammatory disease. Nat. Med. 21, 263–269 (2015). [PubMed: 25686106]
36. Balsinde J, Balboa MA & Dennis EA Inflammatory activation of arachidonic acid signaling in murine P388D1 macrophages via sphingomyelin synthesis. J. Biol. Chem. 272, 20373–20377 (1997). [PubMed: 9252342]
37. Zhao L et al. Selective interleukin-12 synthesis defect in 12/15-lipoxygenase-deficient macrophages associated with reduced atherosclerosis in a mouse model of familial hypercholesterolemia. J. Biol. Chem. 277, 35350–35356 (2002). [PubMed: 12122008]
38. Cyrus T et al. Disruption of the 12/15-lipoxygenase gene diminishes atherosclerosis in apo E-deficient mice. J. Clin. Invest. 103, 1597–1604 (1999). [PubMed: 10359569]
39. Threapleton DE et al. Dietary fibre intake and risk of cardiovascular disease: systematic review and meta-analysis. BMJ 347, f6879 (2013). [PubMed: 24355537]
40. Marques FZ et al. High-fiber diet and acetate supplementation change the gut microbiota and prevent the development of hypertension and heart failure in hypertensive mice. Circulation 135, 964–977 (2017). [PubMed: 27927713]
41. Rivière A, Selak M, Lantin D, Leroy F & De Vuyst L Bifidobacteria and butyrate-producing colon bacteria: Importance and strategies for their stimulation in the human gut. Front. Microbiol. 7, 979 (2016). [PubMed: 27446020]
42. Ait-Oufella H et al. Natural regulatory T cells control the development of atherosclerosis in mice. Nat. Med. 12, 178–180 (2006). [PubMed: 16462800]
43. Kelly CJ, Zheng L, Taylor CT & Colgan SP Crosstalk between Microbiota-Derived Short-Chain Fatty Acids and Intestinal Epithelial HIF Augments Tissue Barrier Function. Cell Host Microbe 17, 662–671 (2015). [PubMed: 25865369]
44. Glover LE, Lee JS & Colgan SP Oxygen metabolism and barrier regulation in the intestinal mucosa. J. Clin. Invest. 126, 3680–88 (2016). [PubMed: 27500494]
45. Riggs MG, Whittaker RG, Neumann JR & Ingram VM n-Butyrate causes histone modification in HeLa and Friend erythroleukaemia cells. Nature 268, 462–464 (1977). [PubMed: 268489]
46. Goodman AL et al. Extensive personal human gut microbiota culture collections characterized and manipulated in gnotobiotic mice. Proc. Natl. Acad. Sci. 108, 6252–6257 (2011). [PubMed: 21436049]
47. McNulty NP et al. The impact of a consortium of fermented milk strains on the gut microbiome of gnotobiotic mice and monozygotic twins. Sci. Transl. Med. 3, 106ra106 (2011).
48. Rey FE et al. Metabolic niche of a prominent sulfate-reducing human gut bacterium. Proc. Natl. Acad. Sci. 110, 13582–13587 (2013). [PubMed: 23898195]
49. Krautkramer KA et al. Diet-Microbiota Interactions Mediate Global Epigenetic Programming in Multiple Host Tissues. Mol. Cell 64, 982–992 (2016). [PubMed: 27889451]

Author Manuscript Author Manuscript Author Manuscript Author Manuscript

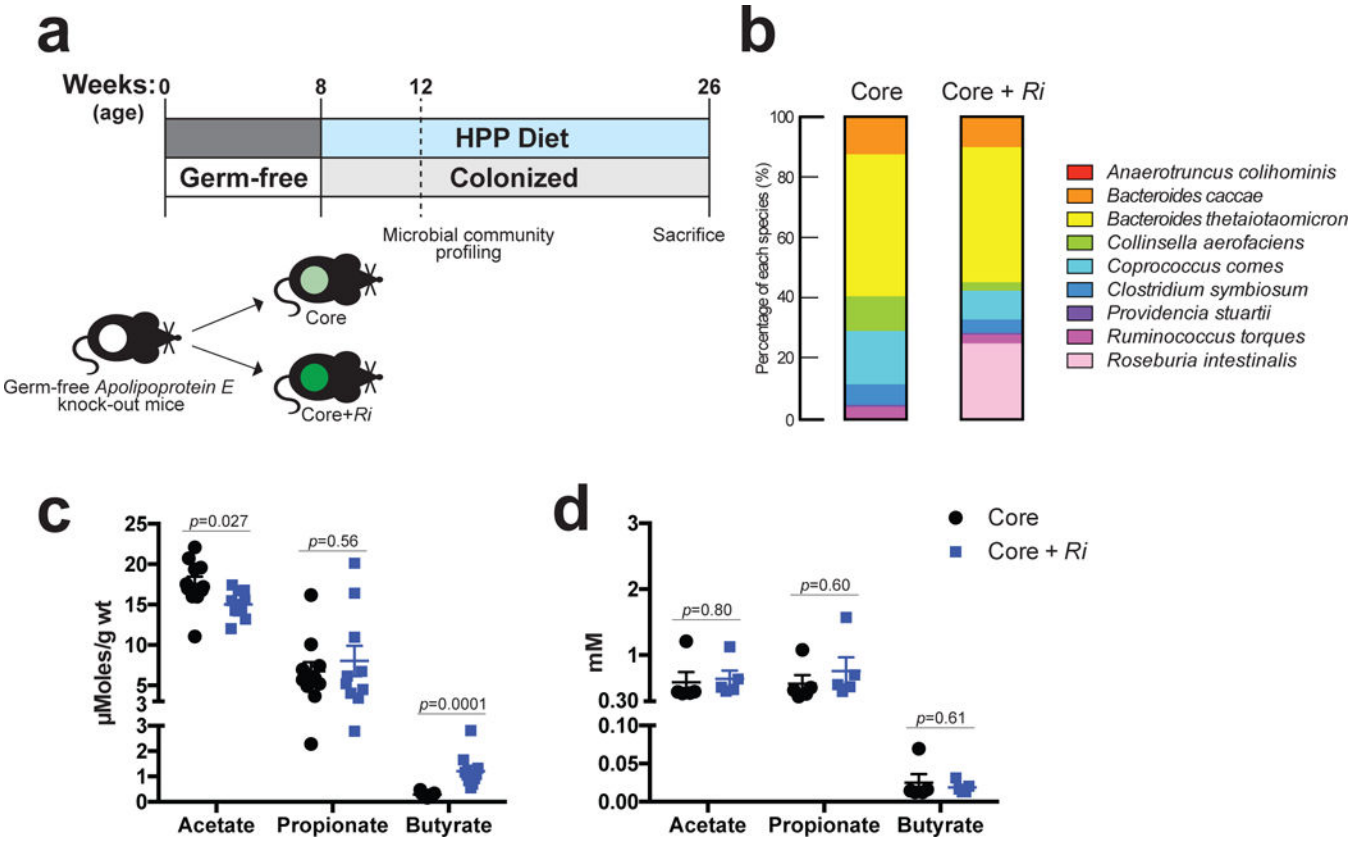

Figure 1. Colonization with *R. intestinalis* increases cecal levels of short chain fatty acids (SCFAs) in mice fed a high plant polysaccharide (HPP) diet.

a, Experimental design. **b**, COPRO-Seq (*co*mmunity *pro*filing by *seq*uencing) analysis of fecal samples from gnotobiotic *Apolipoprotein E* knock-out mice colonized with the "core" community (n=5) or the "core plus *R. intestinalis*" community (n=5). The bar charts show the abundance of each species in each community. **c**,**d**, Levels of SCFAs in cecum (**c**, n=11 in the "core" group and n=10 in the "core plus *R. intestinalis*" group) and plasma (**d**, n=5 per group) in the "core" group and the "core plus *R. intestinalis*" colonized mice assessed by gas chromatography-mass spectrometry. Cecal SCFA levels are indicated by micromoles per gram wet weight (wt). Symbols represent values for individual animals, with averages (horizontal line) plus standard errors of the means indicated. Significance was calculated by an unpaired two-tailed Student's *t* test.

Author Manuscript
Author Manuscript
Author Manuscript
Author Manuscript

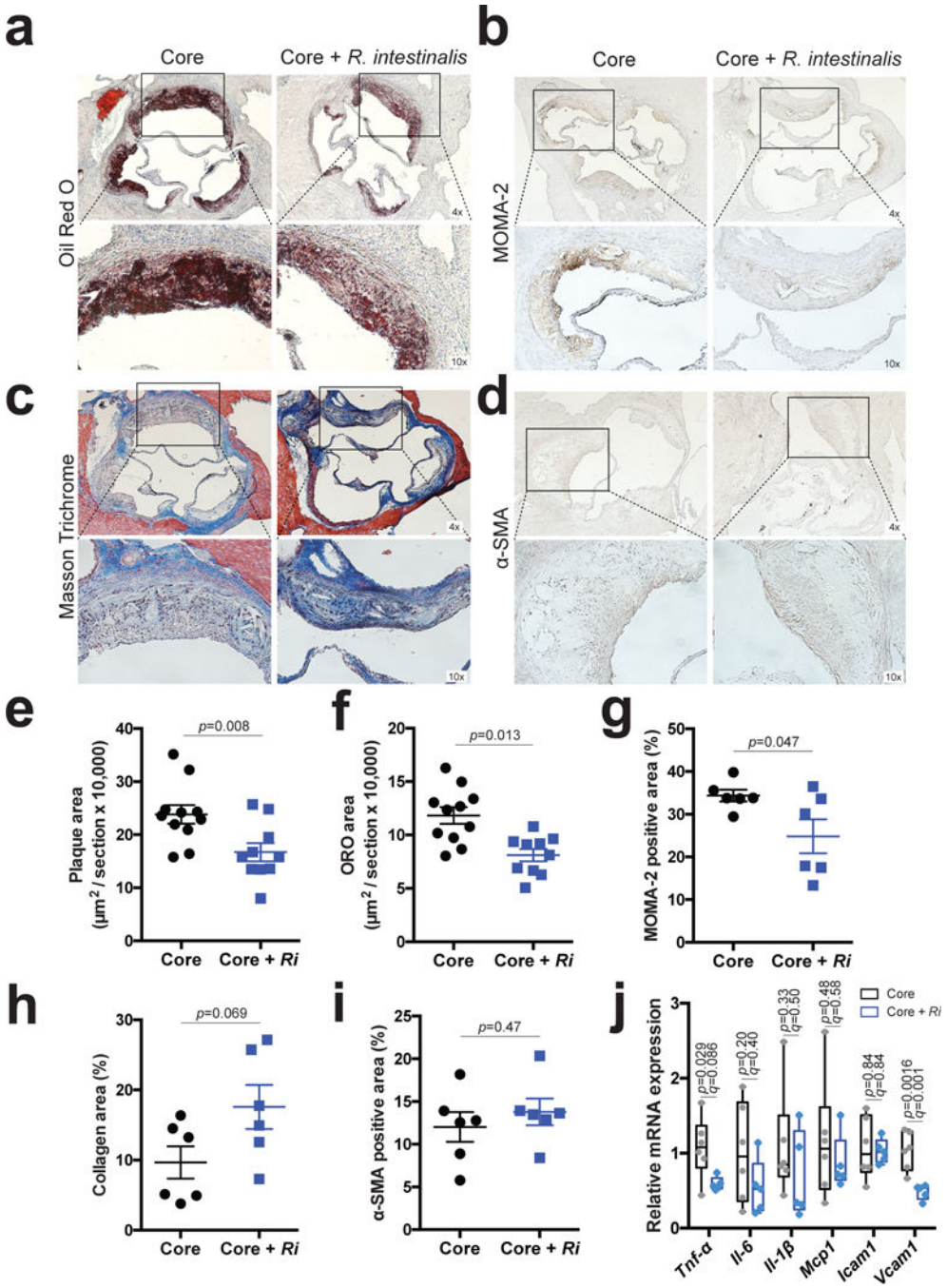

Figure 2. Colonization with *R. intestinalis* inhibits the development of atherosclerosis in mice fed a HPP diet.

a,**e**,**f**, Representative photographs of Oil Red O staining (**a**) and quantitative analysis of plaque area (**e**) and Oil Red O (ORO) positive area (**f**) in the aortic sinus (n=11 in the "core" group and n=10 in the "core plus *R. intestinalis*" group). **b-d**,**g-i**, Representative sections and quantitative analyses of MOMA-2 positive macrophages (**b**,**g**), collagen (**c**,**h**), and α-actin^{+} smooth muscle (α-SMA) cells (**d**,**i**) in the aortic sinus (n=6 per group). Box areas are enlarged below (**a-d**). Symbols represent values for individual animals, with averages

Author Manuscript Author Manuscript Author Manuscript Author Manuscript

(horizontal line) plus standard errors of the means indicated. Significance was calculated by an unpaired two-tailed Student's *t* test. **j**, Gene expression of *Tnf-α*, *Il-6*, *Il-1β*, *Mcp1*, *Icam1*, and *Vcam1* in the aorta from mice colonized with the core" community (n=6) or the "core plus *R. intestinalis*" community (n=5). The data are expressed as box-and-whisker plots where boxes represent median values and interquartile ranges and whiskers represent minimum and maximum values. Significance was calculated by an unpaired two-tailed Student's *t* test, followed by the Benjamini-Hochberg procedure to control the false discovery rate. Gene expression of *Tnf-α* and *Vcam1* showed statistical significance (*q* value of<0.10).

Author Manuscript Author Manuscript Author Manuscript Author Manuscript

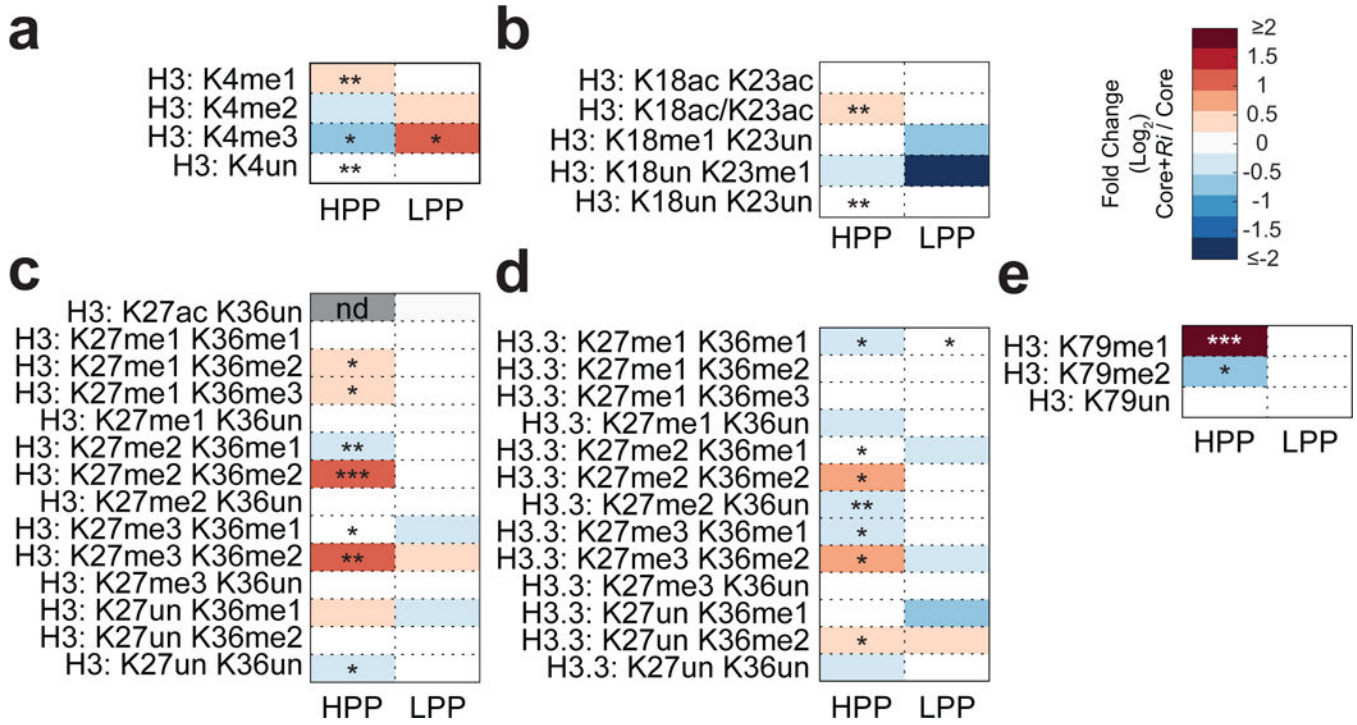

Figure 3. *R. intestinalis* affects histone post-translation modifications (PTMs) in the colon.

Relative abundance of histone PTMs on H3 and H3.3. **a**-**e**, K4 methylation on H3 (**a**), K18 and K23 acetylation and methylation on H3 (**b**), K27 and K36 methylation on H3 (**c**) and H3.3 (**d**), and K79 methylation on H3 (**e**) in the proximal colon. Values are reported as a fold change in "core plus *R. intestinalis*" colon relative to "core" control (n=4 in the "core" group and n=5 in the "core plus *R. intestinalis*" group) for both diets. Significance was calculated by a two-tailed Welch's T-test as follows: *, *P* value of <0.05; **, *P* value of <0.01; ***, *P* value of <0.001. Actual *P* values are found in Supplementary Table 8. HPP and LPP indicate high plant polysaccharide and low plant polysaccharide, and ac, me, and un indicate acetylation, methylation, and unmodified, respectively. For example, H3:K4me3 indicates the trimethylation of lysine 4 of H3.

Author Manuscript Author Manuscript Author Manuscript Author Manuscript

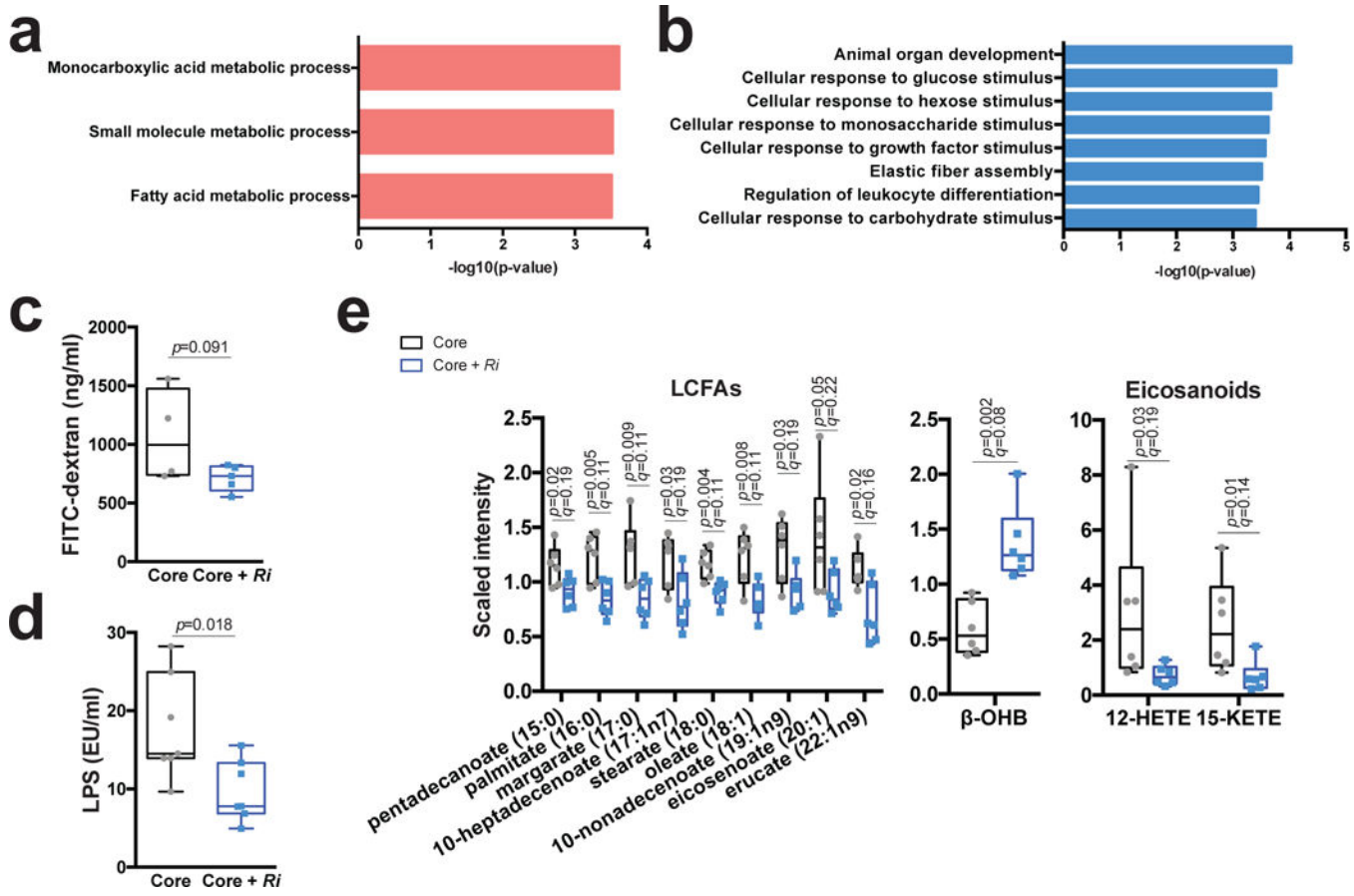

Figure 4. Colonization with *R. intestinalis* regulates energy metabolism and improves intestinal barrier function.

a,**b**, Gene ontology (GO) term enrichments with Fisher's Exact Tests for genes upregulated (**a**) and downregulated (**b**) from RNA-seq analysis in colon samples of HPP diet-fed mice colonized with the "core plus *R. intestinalis*" community (n=5) relative to the "core" community (n=3). **c**, Fluorescein isothiocyanate (FITC) -dextran assay in HPP diet-fed mice colonized with the "core" (n=4) or the "core plus *R. intestinalis*" (n=5). **d**, Plasma LPS levels (EU/ml) measured in mice colonized with the core" community (n=7) or the "core plus *R. intestinalis*" community (n=7). Significance was calculated by an unpaired two-tailed Student's *t* test and the data are expressed as box-and-whisker plots where boxes represent median values and interquartile ranges and whiskers represent minimum and maximum values (**c**,**d**). **e**, Untargeted metabolome analysis of plasma (n=6 per group). Relative mass spectrometry scaled intensities of long chain fatty acids (LCFAs), β-hydroxybutyrate (β-OHB), and eicosanoids detected at significantly different levels between mice colonized with "core" vs "core plus *R. intestinalis*" community (all indicated differences significant at $P<0.05$). Significance was calculated by two-tailed Welch's T-tests, followed by the Benjamini-Hochberg procedure to control the false discovery rate, and the data are expressed as box-and-whisker plots where boxes represent median values and interquartile ranges and whiskers represent minimum and maximum values. 12-HETE and 15-KETE indicate 12-hydroxyeicosatetraenoic acid and 15-ketoeicosatetraenoic acid, respectively.

Author Manuscript Author Manuscript Author Manuscript Author Manuscript

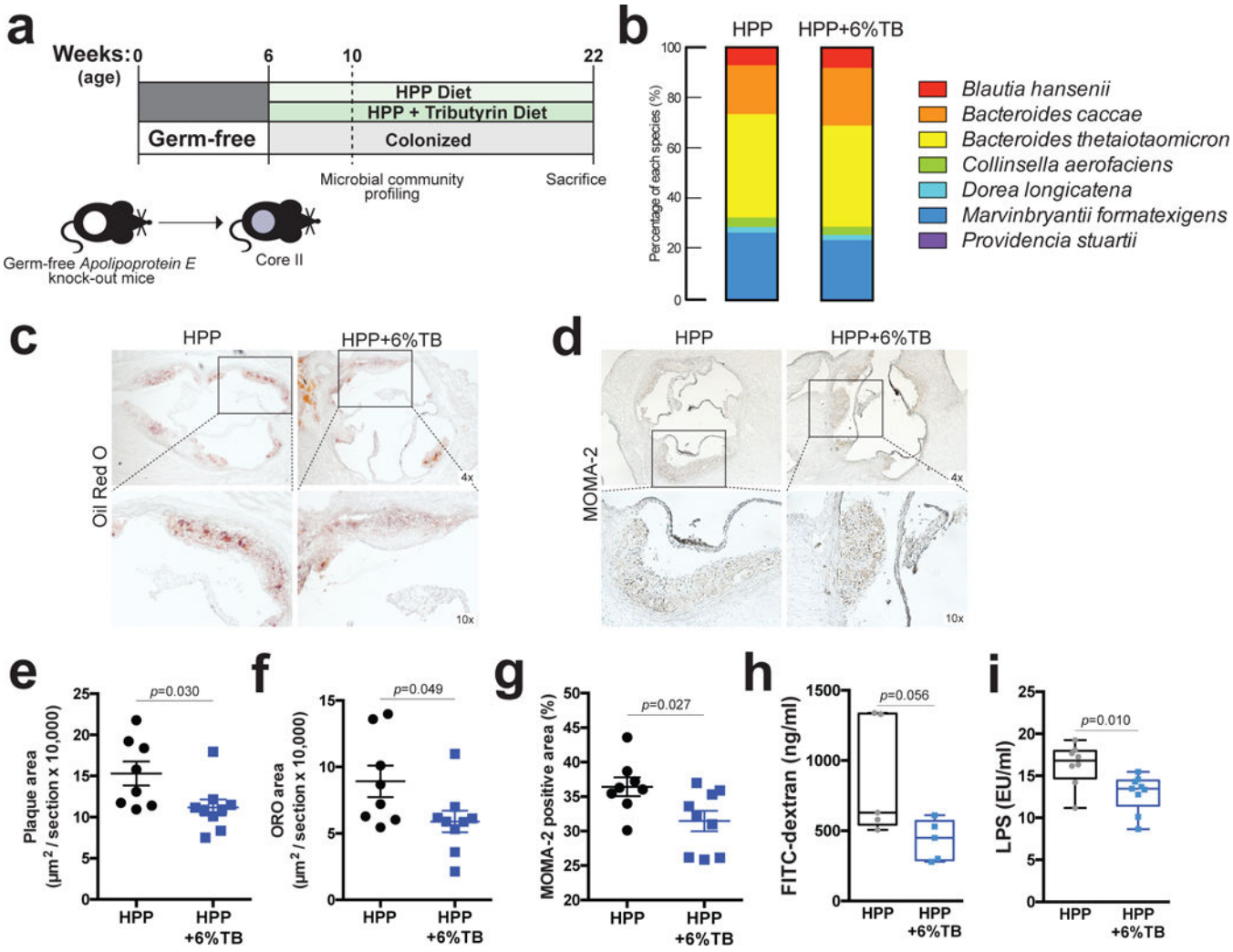

Figure 5. Tributyrin supplementation reduces the development of atherosclerosis in mice colonized with non-butyrate producers.

a, Experimental design. **b**, COPRO-Seq (*co*mmunity *pro*filing by *seq*uencing) analysis of fecal samples from gnotobiotic *ApoE*$^{-/-}$ mice fed with the HPP diet (n=8) or the 6% tributyrin (TB)-supplemented diet (n=9). The bar charts show the abundance of each species in the community. **c**,**e**,**f**, Representative photographs of Oil Red O staining (**c**) and quantitative analysis of plaque area (**e**) and Oil Red O (ORO) positive area (**f**) in the aortic sinus (n=8 in the HPP diet group and n=9 in the tributyrin group). **d**,**g**, Representative sections (**d**) and quantitative analysis (**g**) of MOMA-2 positive macrophages in the aortic sinus (n=8 in the HPP diet group and n=9 in the tributyrin group). Box areas are enlarged below (**c**,**d**). **h**, Fluorescein isothiocyanate (FITC) -dextran assay in mice fed the HPP diet (n=5) or the 6% tributyrin-supplemented diet (n=5). **i**, Plasma LPS levels (EU/ml) measured in mice fed the HPP diet (n=8) or the 6% tributyrin-supplemented diet (n=9). The data are expressed as individual dots with mean ± SEM (**e**-**g**) or box-and whisker plots where boxes represent median values and interquartile ranges and whiskers represent minimum and maximum values (**h**,**i**).